Available online at www.sciencedirect.com
ScienceDirect
Catalysis Today 121 (2007) 170–186
CATALYSIS TODAY
www.elsevier.com/locate/cattod

Combining TAP-2 experiments with atomic beam deposition of Pd on quartz particles

Rebecca Fushimi [a], John T. Gleaves [a,*], Gregory Yablonsky [a], Anne Gaffney [b,1], Mike Clark [b], Scott Han [b]

[a] *Department of Chemical Engineering, Washington University, One Brookings Drive, Box 1198, St. Louis, MO 63130, United States*
[b] *Rohm and Haas Company, 727 Norristown Rd, P. O. Box 904, Spring House, PA 19477-0904, United States*

Available online 4 October 2006

Abstract

This paper presents a new approach for precisely tailoring the surface of complex catalytic particles at the atomic level. We describe a new apparatus of original construction that combines an atomic beam deposition (ABD) system with a temporal analysis of products (TAP-2) reactor system. Catalyst samples were prepared by directly adding metal atoms and metal oxide clusters in sub-monolayer amounts to the surface of micron-sized particles. Precise kinetic characterization, (non-steady-state and steady-state) was performed using pulse response methods, temperature-programmed reaction (TPR), etc.

The new approach is illustrated by the example of CO oxidation over a series of Pd/PdO catalysts. Catalysts of different loadings were prepared by direct atomic deposition on quartz particles. The Pd deposits were characterized using XPS, SEM and TEM. CO_2 production during TPR experiments exhibited oscillatory behavior. The goal of combining ABD with TAP experiments is to develop a method of establishing direct, reproducible correlations between changes in surface composition and changes in catalyst activity.

Keywords: TAP kinetic characterization; Atomic beam deposition; CO oxidation; Oscillatory behavior; Palladium catalysts

1. Introduction

The enormous wealth of kinetic and structural information from studies of model and practical catalytic systems has greatly increased our understanding of the link between catalyst structure and performance. Starting the development of a new catalyst a researcher can draw on this vast reservoir of knowledge, and immediately identify a number of compositions as potential candidates. In many cases, the active bulk phase of a potential candidate has been identified, and its performance has been measured, usually under steady-state conditions. For a number of important practical systems careful kinetic studies using steady- and non-steady-state techniques have been performed yielding rate parameters, and important details of the catalytic reaction mechanism. For a number of model systems, combined surface science and kinetic studies have provided the direct link between surface structure and performance.

The development of practical catalysts such as supported metals or metal oxides often involves a multi-step bulk preparation procedure followed by surface activation. Many practical catalysts contain more than one transition metal, which may exist in different oxidation states. Notwithstanding significant advances in understanding fundamental catalytic processes, practical catalyst development is hampered by a lack of fundamental information relating the surface composition of the catalytic phase and catalyst performance. The surface of a practical catalyst is likely to be compositionally different from the bulk, structurally and compositionally non-uniform, and may change during the course of a catalytic reaction. As a result, information gleaned from determining the bulk crystal structure of a catalyst is of limited value in characterizing a catalyst surface. The chemical properties of a surface may also be strongly influenced by various adspecies, which in turn may change during the course of a reaction. Adspecies, reaction intermediates, and adsorbed reaction products often have short

* Corresponding author. Tel.: +1 314 935 4159.
E-mail address: klatu_00@che.wustl.edu (J.T. Gleaves).
[1] Present address: ABB Lummus Global Inc. 1515 Broad Street Bloomfield, NJ 07003.

0920-5861/$ – see front matter
doi:10.1016/j.cattod.2006.07.061

surface lifetimes, and may exist in low concentration on the surface. As a result, they are difficult to detect and characterize under reaction conditions. Also, the catalytic sites on a practical catalyst may occupy only a fraction of the total catalyst surface making their identification difficult even with surface sensitive techniques. These factors pose serious obstacles to the direct observation and characterization of catalytic sites, and as a result it is difficult to develop detailed structure–activity correlations on practical catalysts.At present, it is not possible to predict how a change in the bulk preparation procedure will affect the surface structure and composition, and/or predict which will give the highest selectivity. During the last decade, the inability to predict the dependence of yield/selectivity on surface composition gave rise to ''combinatorial synthesis and evaluation techniques'' in catalyst development research. These techniques, which are a manifestation of the Edisonian approach, can dramatically increase the rate at which new compositions can be prepared and evaluated, and potentially the rate of catalyst discovery, but may not provide a direct link between surface composition and performance.

The emphasis of experimental surface science has been the development and application of techniques to determine surface composition and structure. A common approach in catalytic surface science is to carefully fabricate a model catalyst to obtain a well-defined surface. After preparation the surface structure is precisely characterized, often with atomic precision, exposed to a reactant or reactants, and the kinetics of the gas–surface interactions are obtained. The ability to obtain precise structural information offers the possibility to establish an unambiguous link between structure and kinetics. When a surface is not well-defined determining a direct link between structure and kinetics is not as straightforward.

In this paper we approach the issue of structure determination from a different direction. We start with an ill-defined material and explore the possibility of using kinetic information to infer structure.

The experimental methodology used in this study follows an approach we call ''interrogative kinetics''. Interrogative kinetics is based on the application of TAP pulse response experiments [1–6] in conjunction with traditional kinetic measurements (steady-state, TPD, step-transient, etc.). Typically a battery of kinetic measurements are used to probe the kinetic characteristics of a catalytic surface, and to monitor how those characteristics change in response to changing reaction conditions (pressure, temperature, surface coverage, reactant composition, etc.).

Interrogative kinetics (IK) involves two types of experiments that are performed in sequence to reveal complex mechanisms and structure–activity relationships. The first type is a ''state-defining'' experiment that does not significantly perturb the kinetic state of the catalyst, but provides intrinsic kinetic information that can characterize the state. TAP Knudsen pulse response experiments, and especially TAP pump-probe experiments can be performed under state-defining conditions.

The second type is a ''state-altering'' experiment, which causes a significant change in the composition and/or structure of a catalyst. Conventional atmospheric pressure transient experiments are state altering, but often cause non-uniform changes in the catalyst composition. The uniform addition or removal of atoms from a catalyst surface is a more useful experiment. Oxygen can be directly added to the surface of a catalyst by heating the catalyst in an oxygen atmosphere. It can also be removed by reducing the catalyst with hydrogen, CO, or a hydrocarbon. Of course oxidation or reduction of a material may initiate a phase change in the surface structure, as well as a change in the surface composition. More challenging than adding oxygen is how to change the metal atom composition of a surface. The direct addition of metal atoms is preferable. In this case, a change in kinetics can be directly attributed to the addition of the atoms.

In this paper we follow the evolution of Pd/SiO_2 catalysts from their initial formation until they are operating under steady-state conditions. We describe a new approach for directly adding metal atoms and metal oxide clusters in sub-monolayer amounts to the surface of micron-sized particles (catalysts or support particles) using atomic beam deposition (ABD). This approach offers the possibility of precisely tailoring the surface of complex particles at the atomic level.

In our experiments, different amounts of Pd and PdO were deposited on quartz particles, and the reactivity of the resulting materials toward O_2 and CO conversion to CO_2 was characterized using TAP pulse response, pulsed temperature-programmed reaction, and steady-state experiments.

2. Motivation for atomic beam deposition

In theory, the direct deposition of atomic species is the most straightforward way of adding atoms to the surface of a particle. In practice however, precursor molecules (e.g., organometallic compounds), which can be thermally decomposed are usually used to deposit metals. Schwarz et al. [7] have reviewed the various impregnation techniques, chemical vapor deposition (CVD), and similar techniques for mounting metal precursors on a catalyst substrate. A disadvantage of conventional mounting techniques is that they generally involve a sequence of complex processes, many of which, are not completely understood [7,8].

Direct deposition of atoms eliminates processes associated with the adsorption and decomposition of precursor molecules. The metal atom concentration of a single catalyst sample can be altered in a stepwise fashion without altering other properties of the sample. Increasing the metal concentration on a single catalyst sample in a series of precise steps and testing the catalytic properties after each step can directly relate changes in performance to the changes in concentration. Similarly, by first changing the metal concentration, then holding it constant while the oxygen concentration is changed, a wide range of catalyst oxidation states for a specific transition metal surface concentration can be analyzed.

Atomic deposition under ultra-high vacuum conditions offers a precise method of delivering metal atoms to a solid surface. With ABD the temperature of the substrate is independent of the beam source, and atoms can be deposited on a cold surface where surface diffusion and activated

chemical reactions are very slow. Consequently, atoms can be added to the surface of a material without disturbing the bulk. Typically atomic beams are used to deposit atoms on single crystals or other planar surfaces [9–22]. To adapt ABD to complex metal oxide particles it is necessary to deposit atoms uniformly among a group of particles.

3. Atomic beam deposition apparatus

Fig. 1 depicts key elements of our atomic beam deposition experiment. Fig. 2 shows a photograph of the actual ABD chamber looking through a view-port during a deposition of copper atoms on a metal oxide catalyst sample. The ABD chamber is a stainless steel cylinder 14 in. in diameter and 20.75 in. high. The chamber is pumped by a 500 l/s turbomolecular pump and a 2500 l/s liquid nitrogen trapped oil diffusion pump. Both pumps can be isolated from the main chamber by means of gate valves. The turbomolecular pump is attached to a 3-in. tube, which is connected to the bottom of the ABD chamber. The tube contains a side port for a mass spectrometer probe. The turbopump gate valve is located between the mass spectrometer and the main chamber, and when it is closed the turbopump maintains the mass spectrometer at vacuum. The diffusion pump is attached to an 8-in. port on the side of the ABD chamber. When the diffusion pump and turbopump gate valves are closed the main chamber can be vented without venting the pumps. During deposition experiments the background pressure in the main chamber is typically 10^{-7} Torr.

The ABD chamber has three 8 in. ports positioned 90° apart centered on a plane that is perpendicular to the cylinder axis. A hinged flange with an 8-in. diameter plexiglass window is attached to the middle port and is sealed with an o-ring. The hinged flange allows rapid access to the ABD chamber and the sample holder. The turnaround time for opening the main chamber and returning to vacuum conditions is about 20 min.

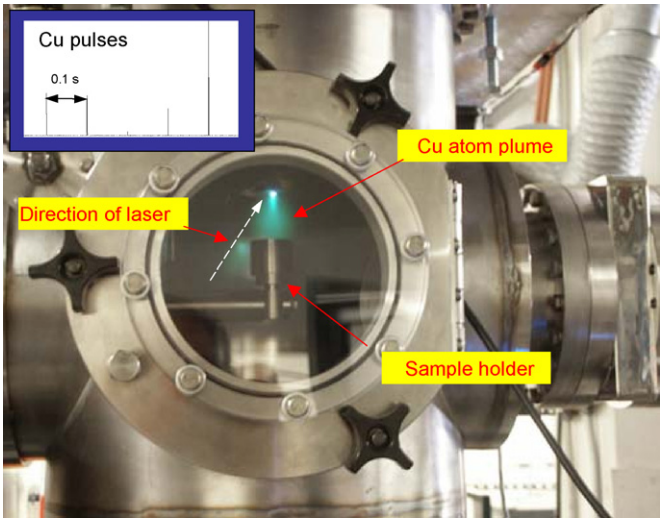

Fig. 2. Atom deposition chamber showing copper atoms being deposited on a metal oxide catalyst. The insert shows the temporal response of $m/e = 63$ (copper atom response) which coincides with the laser pulses. Higher masses were not detected.

The sample holder transport assembly is comprised of a 5-ft long 1-in. tubular arm that enters the ABD chamber through a differentially pumped o-ring fitting. The transport arm passes through an 8-in. stainless steel Tee that is connected to one of the 8-in. ports. The diffusion pump assembly is attached to the bottom flange of the Tee. The transport assembly permits the sample holder to be moved from the ABD chamber to an adjoining vacuum chamber connected to an 8-in. exit port on the opposite side of the chamber. The exit port contains an 8-in. gate valve so that the ABD chamber can be isolated from the adjoining chamber.

Fig. 3 shows side and end-on cross-sectional views of the sample holder assembly. The particle container is cylindrically shaped and has a magnetic diaphragm in the bottom. Sending a

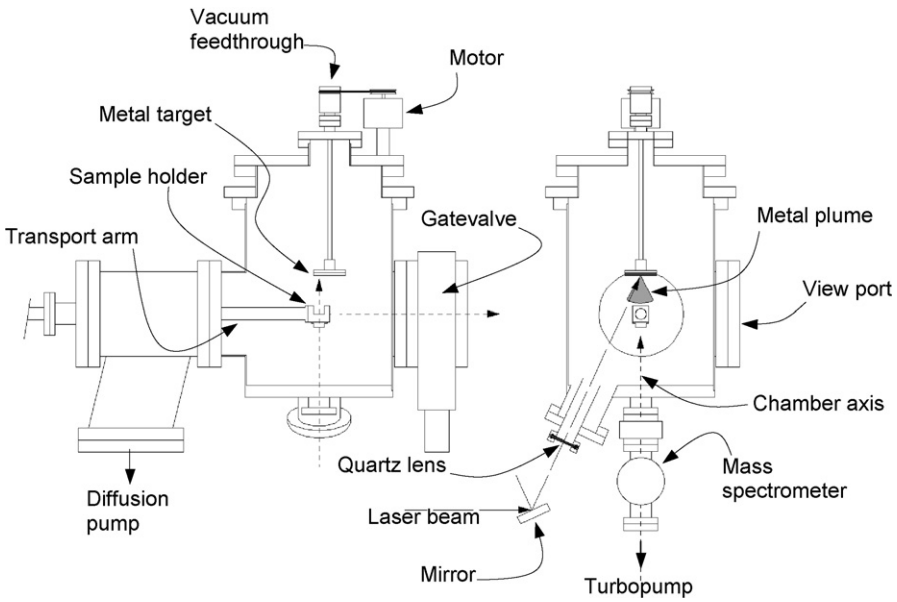

Fig. 1. Key features of atomic beam deposition experiment. Metal atoms are produced by focusing a high-energy laser pulse on a transition metal target. The particle bed is continuously agitated.

pulsing current through the electromagnetic coil causes the diaphragm to vibrate, and the particles to bounce around on the diaphragm surface. Changing the pulsing rate or current changes the frequency and intensity of the vibration, and as a result the strength of particle agitation. Typical frequencies used in deposition experiments ranged from 100 to 5000 Hz. The end-on cross-sectional views show how the particle container, diaphragm, and electromagnet can be rotated to empty particles into a microreactor.

During a deposition experiment the sample holder is positioned in the ABD chamber beneath a metal target. The chamber is evacuated and the particle bed is strongly agitated so that the particles are kept in random motion. Since the mean free path at 10^{-7} Torr is significantly larger than the ABD chamber, atoms produced at the target will undergo collision free travel in straight lines. Approaching the particle bed from above atoms will deposit on any surface that comes in the line of sight of the beam. Strong agitation of the particle bed continuously alters the particle surface presented to the beam of atoms. By varying the atomic flux, the particle bed depth, and the frequency and intensity of the bed vibration the rate and uniformity of coverage can be controlled.

Metal atoms are produced at the metal target by focusing the light from a pulsed excimer laser (Lambda-Physik EMG-100, XeCl active medium 150 mJ pulse energy) onto the surface of the target. Laser ablation has been used extensively to produce atoms, ions, and metal clusters in molecular beam studies, and to produce thin films [23–31], and even metals with high melting points such as tungsten can be deposited. The ablation source used in our deposition system incorporates features of previous designs.

As illustrated in Fig. 1 the laser beam enters the bottom of the ABD chamber through a quartz lens with an 18-in. focal length. The lens is sealed with an o-ring in a telescoping tube assembly, which is used to adjust the beam focus. The beam axis intersects the central axis of the ABD chamber at a 25° angle. The target is mounted on a circular metal plate that is attached to the shaft of a rotatable vacuum feedthrough, which is sealed on the ABD chamber top flange. The feedthrough is connected to a small motor, which allows the shaft, and target to be continuously rotated at speeds ranging from 1 to 20 rpm.

The laser pulse ablates the target surface producing a plume of metal atoms, ions, and metal clusters. The number of atoms produced per pulse depends on the nature of the target material, and on the laser pulse parameters (wavelength, intensity, fluence, pulse duration, etc.) In a typical experiment, a 12 ns 308 nm pulse was focused to a spot size ≈1 mm in diameter. Most experiments were performed using pulse rates between 1 and 20 Hz.

4. Combining ABD with a TAP-2 reactor system

Fig. 4 shows a simplified schematic of the atomic beam deposition system and a TAP-2 reactor system combined into a

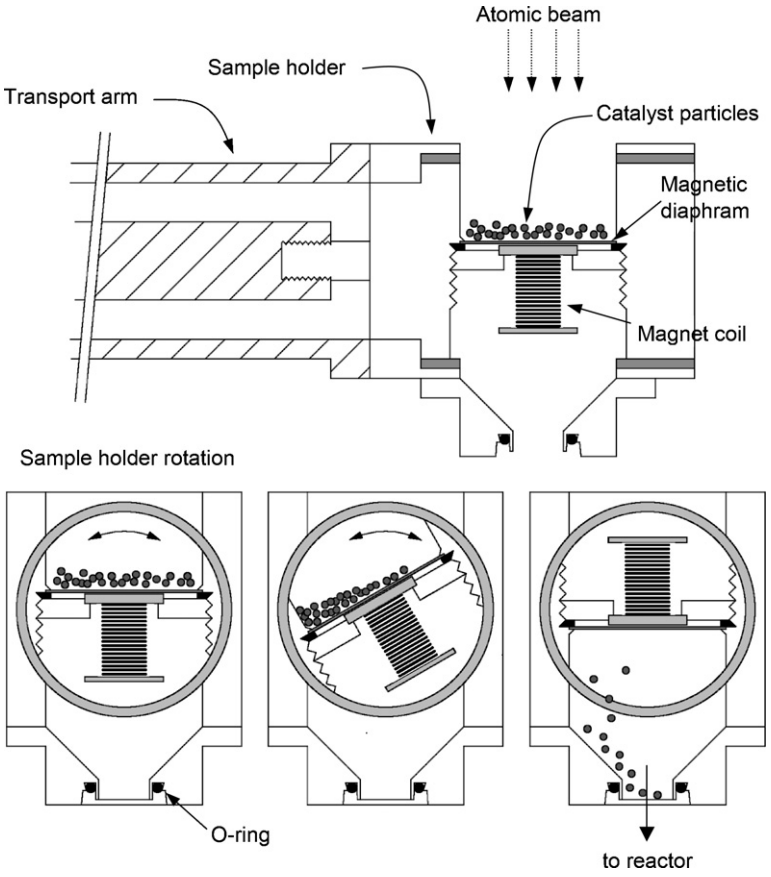

Fig. 3. Cross-sectional views of sample holder assembly.

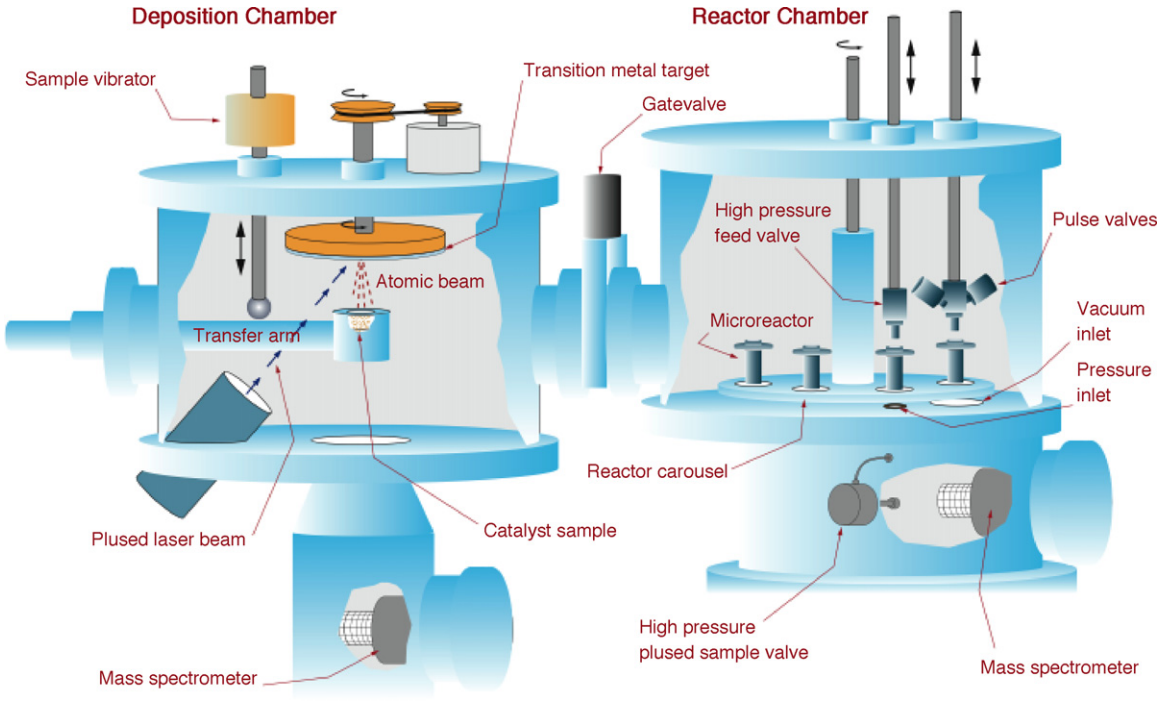

Fig. 4. Simplified schematic representation of combined TAP-2 and atom deposition system. Samples prepared in the atom deposition chamber can be transferred to a TAP microreactor under vacuum conditions.

single apparatus. A photograph of the actual apparatus is shown in Fig. 5. A vacuum gate valve separates the two systems so that they can be operated independently. The deposition process typically takes 5–15 min after which the sample can be transported under vacuum to a microreactor in the TAP system.

The TAP-2 system shown in Fig. 5 is an enhanced version of previous TAP-2 systems. The high-speed vacuum system is comprised of a 30-in. liquid nitrogen trapped chamber pumped by three 10-in. oil diffusion pumps, which have separate adjustable baffles. A 12-in. gate valve separates the liquid nitrogen trap from the mass spectrometer chamber that contains a UTI 100C QMS.

This version of the TAP-2 system has a reactor vacuum chamber, which can be raised and lowered pneumatically giving easy access to the microreactor assemblies. Inside the reactor chamber is a reactor carousel that can hold five individual microreactor assemblies at one time. By rotating the carousel the different microreactors can be positioned under the

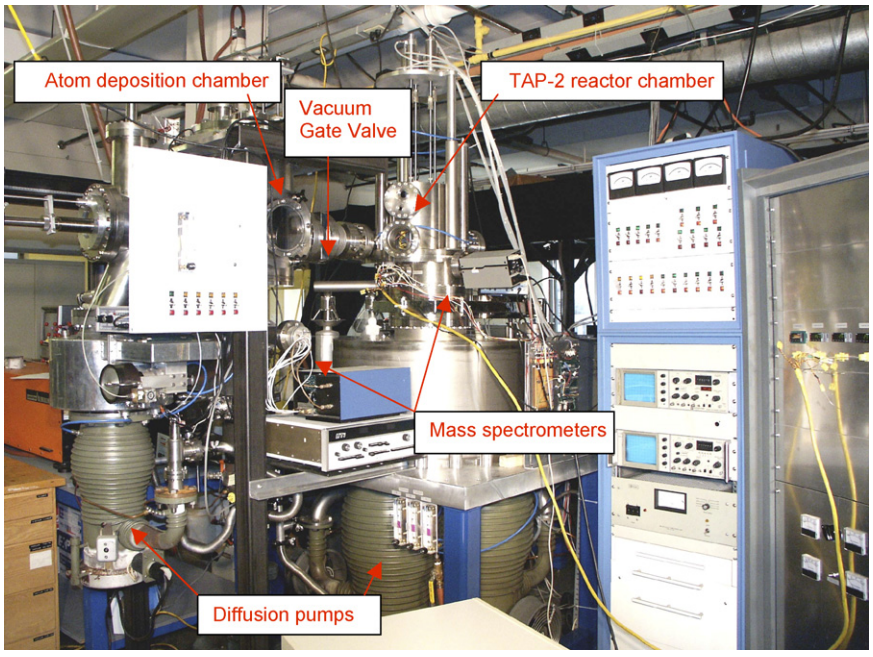

Fig. 5. Combined atom deposition system and TAP-2 multiple reactor system.

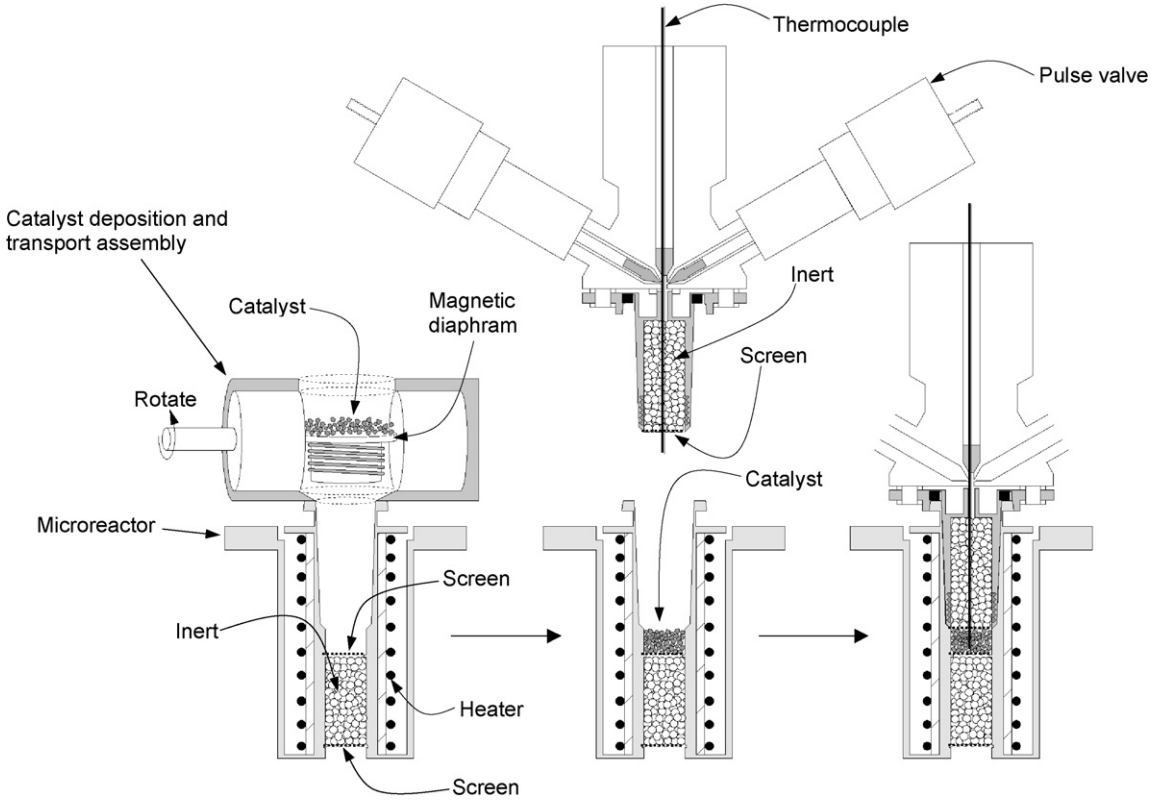

Fig. 6. Detail of the catalyst transfer mechanism which allows samples to be moved between deposition and TAP reactors without exposure to atmosphere.

pulse valve assembly or under the high-pressure flow assembly. Each microreactor can be heated independently, and one reactor can be exposed to vacuum conditions while another is operated at high pressure.

Fig. 6 illustrates how a catalyst formed in the deposition chamber can be transferred to a TAP microreactor without exposing the sample to atmosphere. The microreactor assembly separates into male and female sections each containing a charge of inert particles. The inert particles are held in place between two screens. The upper male section is attached to the pulse valve manifold, and contains a thermocouple for measuring the temperature in the catalyst zone. The female section ''floats'' in a spring-loaded assembly so that as the two halves are joined they self-center. The upper half of the female section contains space for the male section and a small catalyst sample. The two sections are precisely tapered at the same 2.0° angle, and are polished together so that they form a vacuum tight fit when pushed together. As an additional safeguard against a vacuum leak the top section contains an o-ring that seals on the top of the lower section. When the upper and lower halves of the microreactor assembly are joined the remaining empty volume that can be filled with catalyst particles is $\approx 0.125\ cm^3$.

5. TAP vacuum pulse response experiments

TAP vacuum pulse response experiments [32] have been used extensively to study selective oxidation and other types of catalytic reactions on bulk catalysts [1–6,32–95]. The TAP-2 reactor system is an apparatus that is used to perform TAP experiments and other types of non-steady-state and steady-state experiments. The TAP-2 microreactor, which holds the catalyst sample can be easily cycled between vacuum conditions and atmospheric pressures without exposing the catalyst to the atmosphere.

In a TAP experiment catalyst particles are sandwiched between inert particle beds in a small fixed bed microreactor [2,91,93]. One end of the microreactor is attached to a manifold containing one or more high-speed pulse valves, and the other end is attached to an ultra-high vacuum system that has a very high pumping speed.

Introducing one or more very short pulses of reactant gas into the evacuated microreactor performs a standard TAP experiment. The separation between pulses is usually made longer than the time it takes the gas from one pulse to exit the microreactor. The reactor may be operated isothermally or may be temperature programmed.

The time-dependent gas flow [molecule/s] that escapes the microreactor is measured by a mass spectrometer, which makes it possible to measure very small signals with precise time resolution. A single pulse is typically very small ($\approx 10^{-10}$ to 10^{-8} mol/pulse), and gas transport through the particle bed occurs by Knudsen diffusion. The number of molecules per pulse is usually much smaller than the total number of active sites in the catalyst, and reaction of a single pulse typically changes the catalyst composition by less than 0.1%.

Injecting a large number of low intensity pulses over a small catalyst sample performs a TAP titration experiment. The

titration experiment can be used to oxidize or reduce a catalyst and the amount of reactant consumed or released can be precisely determined. If the catalyst zone is sufficiently thin (less than 10% of the total reactor length) the catalyst composition changes uniformly throughout the catalyst zone even for a very large number (10,000) of pulses (this feature of a TAP "thin-zone" reactor has been discussed in the literature) [1,91,93,94]. The titration experiment can be used to determine the number of active sites under reaction conditions, and how the kinetic characteristics change as the catalyst is oxidized or reduced.

The theoretical basis of TAP experiments is fully developed and well established [1,38,96–100]. TAP pulse response experiments are described by a set of partial differential equations that can be solved analytically using a moment-based analysis [1,38,97]. The general solution contains primary kinetic characteristics (e.g., apparent rate constants, apparent surface residence time, etc.), and these characteristics can be directly and easily calculated from the moments of the experimentally observed exit flow. The primary kinetic characteristics are directly related to the intrinsic catalytic properties (composition, structure) of the catalyst.

6. Experimental results and analysis

Central to our experimental methodology is the measurement of intrinsic kinetic characteristics of a catalyst as the catalyst undergoes a stepwise alteration of one of its components. For example, we have investigated the dependence of kinetic characteristics on the surface oxygen concentration of mixed metal oxide catalysts [1,3,4,33–35,38,39,49,90,94]. In these studies, heating the metal oxide in an oxygen atmosphere or exposing the oxide to a series of oxygen pulses altered the oxygen surface concentration.

Using the IK approach to determine kinetic dependence on surface metal atom concentration requires the surface concentration of one metal be altered in a stepwise fashion. To obtain uniform coverage on irregular particles we devised a simple method of exposing particles to a pulsed metal atom flow. The pulsed flow is created by laser ablation of a metal target, and uniform coverage is obtained by continuously stirring the particles in the flow.

6.1. Atomic deposition on silicon wafers

Laser ablation has been used extensively to deposit metals [23–31] on various substrates to make thin films, and in a number of studies pulsed laser deposition (PLD) has been used to deposit metals on well-defined, two-dimensional crystals [101–106]. For example, Eppler et al. employed PLD for the fabrication of Pt nanoparticles in the size range of 2–50 nm on the surface of a silicon wafer [101]. TEM, AFM, UPS, and SEM were used to characterize the nanoparticles and, despite the low surface area, reaction studies of ethylene hydrogenation demonstrated catalytic activity.

To determine the number of metal atoms per laser pulse, and the approximate number of pulses needed for monolayer coverage we deposited Pd atoms on a number of substrates. Initial normalization tests were performed using a silicon wafer substrate. In a typical experiment, a silicon wafer was positioned in the deposition chamber under the Pd target. The chamber was evacuated to 10^{-6} Torr and the Pd target was exposed to a series of laser pulses (from 1000 to 100,000 pulses). The silicon wafer and the Pd target were maintained at room temperature during pulsing.

The resulting Pd deposits were analyzed using XPS (Kratos Axis-Ultra with a DLD detector source Monochromatic Al–K alpha pass energy for high resolution data collection −20 eV step size −0.05 eV) to determine the weight percent of deposited palladium.

Fig. 7 shows a typical XPS spectrum of a Pd deposit on a silicon wafer. The deposit contains Pd metal and PdO. The amount of Pd as PdO ranged from 23 to 37.5% of a deposit. Oxide may sputter off the Pd target during deposition, and an oxide layer may form after the Pd is removed from the vacuum chamber, and the sample is exposed to atmospheric pressure.

For samples receiving 10,000 or more laser pulses Pd particles could be directly observed. The particles were imaged using a JEOL 6700 FESEM. On the intermediate sample with 8000 laser pulses, a wide size distribution of deposits was found ranging in diameter from <10 nm to 2 μm. Fig. 8 shows deposits are generally round, with some evidence of crystallinity with slightly linear edges and a possible diffraction pattern. Particle composition was analyzed using a PGT-Prism2000 EDS system. Performed in spot mode, the major impurities present were (in descending order) Au, Cu, Mg, and Al.

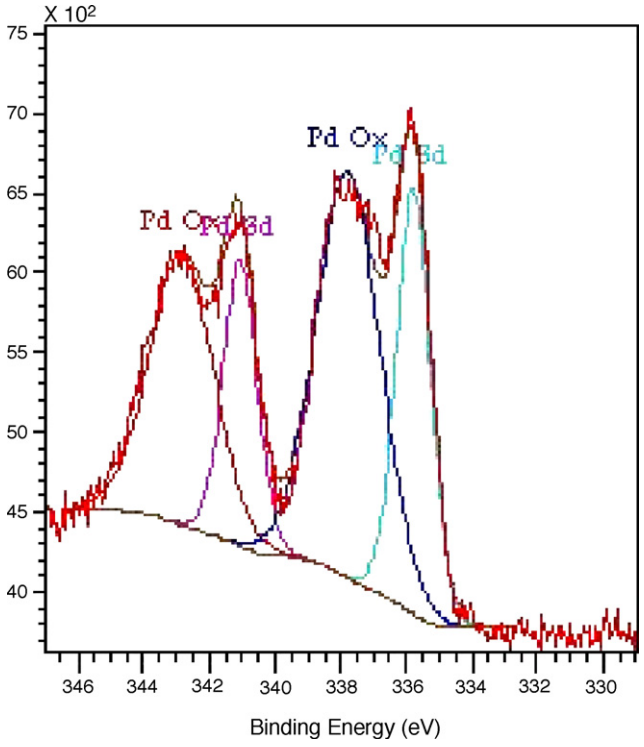

Fig. 7. XPS of an intermediate palladium deposition loading, Pd = 8000 pulses on a silicon wafer.

Fig. 8. FESEM images of palladium (Pd loading = 8000 pulses) deposited on silicon showing a 30 nm particle. Particles <5 nm are clearly evident.

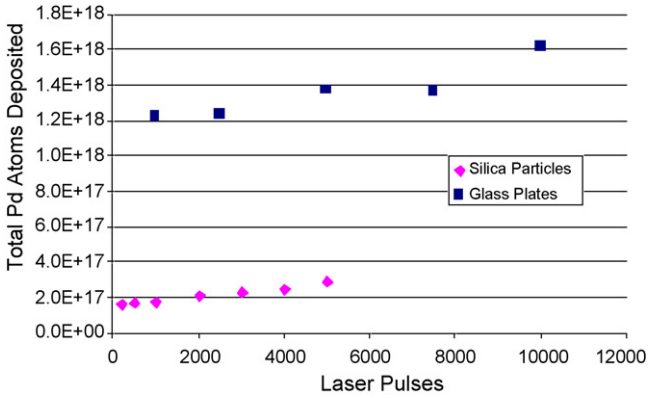

Fig. 9. Number of palladium atoms added at various deposition durations on silica particles and glass plates.

6.2. Atomic deposition on SiO_2 particles

Using the silicon wafer results as a guide a series of Pd/SiO_2 catalyst samples were prepared by depositing Pd atoms on 210–250 μm quartz particles. The structure of Pd deposits on SiO_2 particles is expected to differ from that of deposits detected on Si single crystals due to differences in surface wetting. However, it is reasonable to assume that similar palladium loadings are achieved at the same deposition conditions (e.g., laser pulse intensity, number of laser pulses, etc).

In a typical experiment, a sample of quartz particles was positioned in the deposition chamber under the Pd target. The chamber was evacuated to 10^{-6} Torr and the Pd target was exposed to a series of laser pulses (from 500 to 100,000 pulses). The quartz substrate and the Pd target were maintained at room temperature, and the particles were continuously agitated during pulsing.

The palladium deposits were characterized using XPS, SEM, and TEM. Samples prepared using 100,000 laser pulses gave an XPS palladium signal that was variable but generally readily apparent. The Pd and PdO spectra resembled that of deposits on the silicon substrate. SEM–EDS mapping did not resolve any particles indicating that the palladium deposits were <100 nm in diameter and likely below the 10 nm range. On samples prepared with 10,000 laser pulses the Pd signal was weak or not detectable. Pd could not be detected on samples prepared with 5000 laser pulses or less using XPS.

A more quantitative measurement of the total number of palladium atoms added during the deposition was made using inductively coupled plasma mass spectrometry (ICPMS). After depositing palladium on the surface of silica particles (the same material used as a catalyst support), the metal was removed by soaking the particles in hot sulfuric acid overnight. PdO is insoluble in H_2SO_4 and was not measured in this analysis. This solution was then analyzed with ICPMS. In a similar fashion the depositions were repeated on a series of glass plates. The plates were soaked in hot sulfuric acid and the solution analyzed. Fig. 9 shows the number of palladium atoms added as the number of laser pulses increases on both the silica particles and the glass plate substrate.

In general, the total loading was an order of magnitude higher on the two-dimensional substrate compared to the three-dimensional particle deposition. This is expected since a portion of the beam may be lost through the bed as it is agitated, with deposition on a two-dimensional surface the entire beam is intercepted. Note that the trend in deposition does not pass through zero. It is expected that the initial laser pulses (∼500 pulses) are of much greater intensity which quickly drop off in a non-linear fashion. Thus a great amount of material is deposited early in the deposition. After this initial deposition, the amount of deposited material increases linearly with the number of laser pulses.

6.3. Combining deposition experiments with TAP experiments

It is well known that in many catalytic systems the reaction mixture changes the catalyst. For example, with multi-component metal oxide catalysts the reaction mixture can cause a surface enrichment of one component over another. In catalysts containing a single component, the reaction mixture can cause a change in the surface structure. In either case, interaction with the reaction mixture can cause a change in catalytic reactivity.

When a catalytic reaction is performed at steady-state conditions it is assumed that the catalyst composition is constant. Under steady-state conditions the catalyst composition can be viewed as an ‘‘end-state’’, which results from exposing the catalyst to a reaction mixture for the period of time required to achieve a steady-state yield. A catalyst in such an end-state is often called ‘‘reactor-equilibrated’’. The advantage of steady-state operation is reproducibility, and correspondence to industrial operation. The disadvantage is loss of information about different kinetic states, and the difficulty of determining intrinsic kinetic characteristics.

Advantages of non-steady-state techniques are the ability to determine the kinetic characteristics of different kinetic states, the ability to measure intrinsic kinetic characteristics, the ability to provide detailed mechanistic information (including the nature of short-lived reaction intermediates), and the ability to track the evolution of catalytic properties as a material changes.

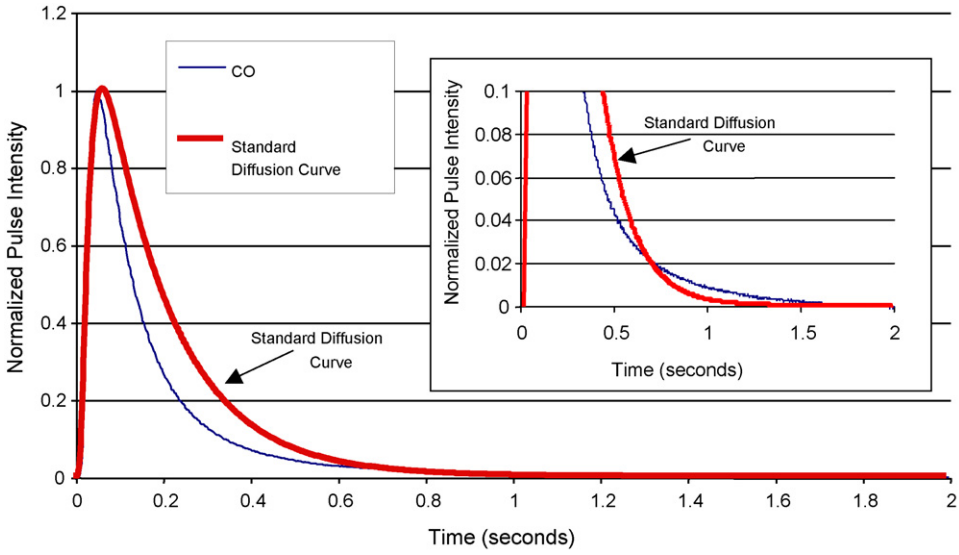

Fig. 10. Exit flow of CO pulsed over a fresh catalyst AB0.85 (850 Pd pulses) at 20 °C compared with the theoretical standard diffusion curve. The inset shows the two curves crossover one another.

However, non-steady-state testing often leads to irreversible changes, and experimental conditions that are difficult to reproduce. To overcome these disadvantages, the IK methodology attempts to develop cyclic experiments in which a catalyst state is altered and then regenerated. An example of an interrogative kinetic cycle would be the reduction of an oxide surface by pulsed reduction with a reactant (e.g., CO, alkane, alkene) followed by re-oxidation. If after re-oxidation the same kinetic properties are obtained we can conclude that the original kinetic state has been restored. If the initial state cannot be regenerated we can conclude that the structure of the catalyst has changed irreversibly. Thus, by using cyclic experiments we can determine changes in structure from kinetic information alone.

In the remainder of this section we describe the battery of kinetic experiments performed in a TAP-2 reactor on a series of Pd/SiO_2 catalysts in the sequence the experiments were performed. Data is shown as pulse response curves, multipulse experiments, or the integral of multipulse response experiments indicating total amount of species consumed. The goal of combining ABD with TAP experiments is to develop a method of establishing direct, reproducible correlations between changes in surface composition and changes in catalyst activity.

As previously described Pd samples were prepared in vacuum and then exposed to air before being transferred to the TAP-2 reactor or analyzed for Pd coverage. In future work, we will discuss transfer made under vacuum. All samples were packed in a thin-zone configuration between two zones of inert quartz particles (210–250 μm). After loading, the microreactor was placed on the input port of the TAP mass spectrometer chamber, and the reactor input was sealed against the pulse-valve manifold. The reactor was then evacuated, and the evacuation mass spectrum was recorded. The main desorption product was water.

6.3.1. TAP Knudsen pulse response experiments on fresh Pd samples

After evacuation the catalyst was exposed to a short series of pulses containing a one to one mixture of CO/Ar or a one to one mixture of O_2/Ar at the room temperature. The response curves of CO and O_2 versus a standard diffusion curve are plotted in Figs. 10 and 11, respectively. Fig. 10 shows that at short times the CO response is narrower than a standard diffusion curve (STD). At 0.75 s the CO response crosses the STD and decays more slowly. This behavior indicates reversible adsorption [2]. An estimation of the equilibrium constant, $K_{eq} = (k_a/k_d)$ for reversible adsorption gives a value ≈2, where k_a and k_d are the constants of adsorption and desorption, respectively. Fig. 11 shows that the O_2 pulse response curve does not differ significantly from a standard diffusion curve. Thus oxygen behaves much like an inert gas and oxygen adsorption is negligible over the freshly deposited material.

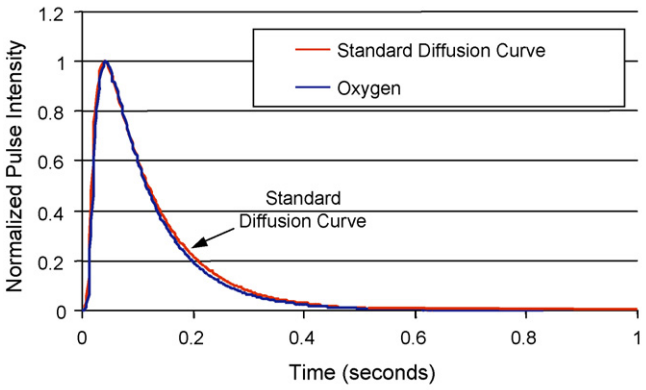

Fig. 11. Exit flow of O_2 pulsed over a fresh catalyst AB0.85 (850 Pd pulses) at 20 °C compared with the theoretical standard diffusion curve.

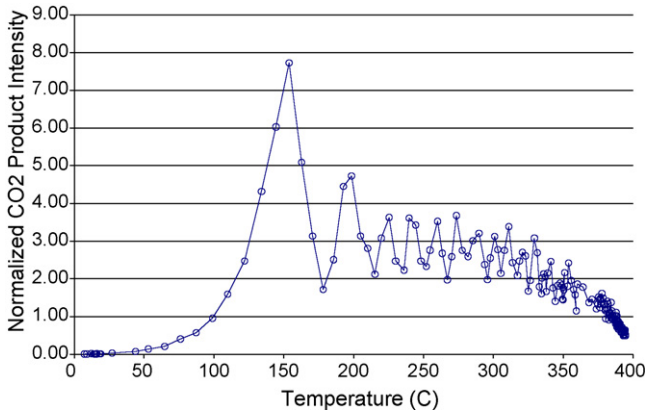

Fig. 12. CO_2 production (determined by measuring the zeroth moment of the CO_2 responses) over fresh deposit AB0.75 (750 Pd pulses) obtained by pulsing CO and ramping the temperature from RT to 400 °C. After the initial maximum the CO_2 response oscillates as the temperature continues to rise.

6.3.2. *Pulsed temperature-programmed reaction (TPR) of fresh Pd samples*

To eliminate the oxygen acquired during catalyst preparation the Pd/PdO/SiO_2 samples were reduced by pulsing CO and ramping the temperature (≈1 °C/s) from 20 to 400 °C. During the temperature ramp the CO, Ar and CO_2 responses were recorded. Oxygen uptake was performed at low temperature to prevent migration in the catalyst bulk. CO was pulsed while ramping the temperature to ensure the removal of added oxygen via reaction rather than migration into the bulk.

Fig. 12 shows CO_2 production as a function of temperature over a sample (AB0.75) containing 750 Pd pulses. A maximum in CO_2 production is observed at 154 °C. After the maximum, production drops rapidly as the sample continues to heat. The initial steep drop in CO_2 production is followed by a gradual decrease with periodic bursts giving the appearance of a damped oscillation. All freshly deposited samples exhibited this oscillatory behavior. The reactor temperature was maintained at 400 °C until CO_2 production was <5% of its maximum value. The trend in CO_2 production and the total amount produced was highly reproducible on separate samples prepared with identical Pd loadings.

6.3.3. *Re-oxidation of reduced Pd/SiO_2 samples at 20 °C and TPR*

After CO reduction each Pd/SiO_2 sample was cooled to room temperature and exposed to the long series of oxygen pulses at room temperature. Fig. 13 shows a typical series of oxygen response curves, which were observed over every sample after CO reduction of the fresh material. At the start of the sequence oxygen conversion is 100%. At the end, the oxygen pulse response displays the characteristic shape of a standard diffusion curve.

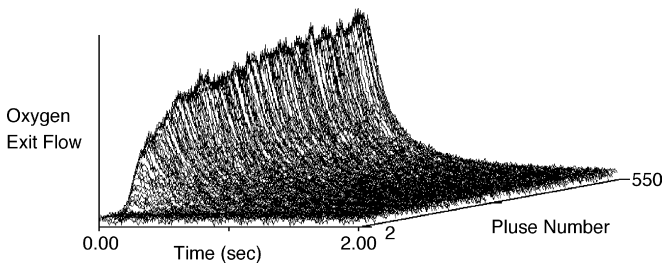

Fig. 13. A series of oxygen pulse response curves obtained at 20 °C over a reduced Pd/SiO_2 catalyst (750 Pd pulses).

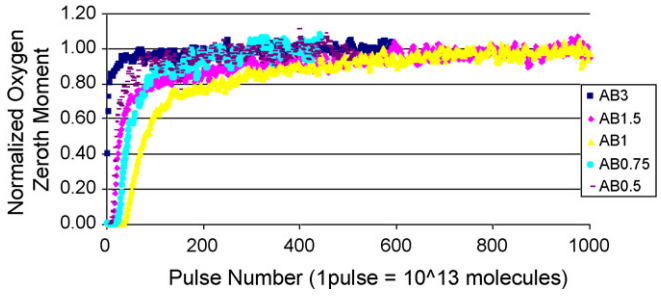

Fig. 14. Oxygen breakthrough curves for a series of reduced Pd/SiO2 samples obtained at 20 °C.

Fig. 14 is a plot of the area under a series of O_2 response curves (the zeroth moment) for a number of different samples with different Pd loadings. The curves have been normalized to the total oxygen pulse intensity, and the pulse number scale is adjusted so that one pulse represents 10^{13} oxygen molecules. The trend in O_2 uptake and the total amount consumed was highly reproducible on separate samples prepared with identical Pd loadings.

For every sample, the total oxygen uptake can be summed pulse-by-pulse, and its value is presented in Fig. 15 versus number of Pd laser pulses. Fig. 15 shows that the total oxygen uptake at 20 °C is not a monotonic function of the number of laser pulses, but follows the total CO_2 production curve recorded during TPR (the integral of Fig. 12), which is also plotted in Fig. 15. This surprising trend indicates that the structure of the material plays a role in these reactions rather than simply the total amount of Pd material. Fig. 16 plots the O_2 uptake at 20 °C versus total CO_2 production for different Pd loadings, and shows a clear linear relation between the two. The total oxygen consumed during room temperature uptake is two orders of magnitude lower then the oxygen removed during the initial CO reduction.

After re-oxidizing each sample at room temperature, the surface was tested for its affinity for CO by pulsing CO at 20 °C.

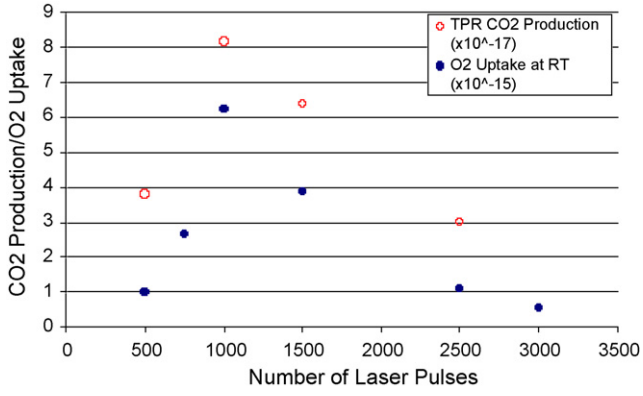

Fig. 15. Total oxygen uptake at 20 °C and total CO_2 production during TPR for different numbers of laser pulses. Oxygen uptake tracks CO_2 production rather than number of laser pulses (the amount of Pd deposited).

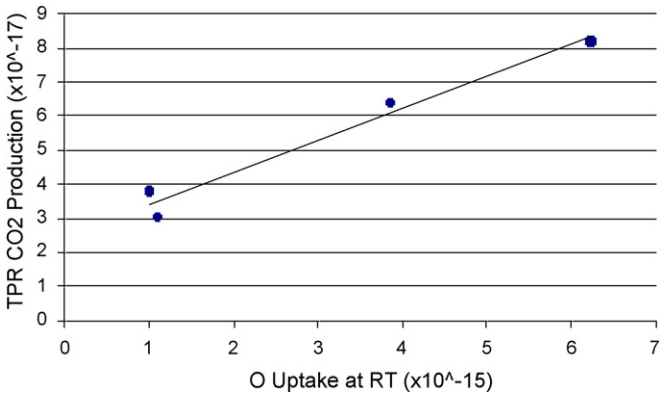

Fig. 16. Total oxygen uptake at 20 °C vs. total CO_2 production for different Pd loadings.

Fig. 17 compares the CO pulse response recorded over the fresh catalyst sample, and that exposed to a CO TPR and oxygen uptake at 20 °C. The change in the adsorption properties is remarkable. Recall that Fig. 10 demonstrated a slight reversible adsorption over the fresh catalyst when compared to the standard diffusion curve. After reducing the catalyst and re-oxidizing at low temperature the adsorption of CO is now strongly reversible indicating a clear structure change has occurred.

The re-oxidized samples were next reduced with a CO TPR in similar manner as the initial surface. The CO_2 production as a function of temperature is displayed in Fig. 18.

The CO_2 production exhibits a smooth rise until the temperature reaches 400 °C. At this point the CO input was halted for ≈10 min, and the catalyst was held in vacuum at 400 °C. The large CO_2 response labeled "restart experiment" is the first pulse observed after restarting the CO input. After this pulse, production drops quickly and then continues to slowly decreases. Total CO_2 production after re-oxidation is ≈10× less than that produced by the fresh samples.

After exposing a re-oxidized sample to a long series of CO pulses at 400 °C the sample was cooled to room temperature and re-oxidized as before. The resulting breakthrough curve is plotted along with the initial breakthrough curve in Fig. 19. The breakthrough curves display identical dependence, and the same number of O atoms is consumed in both cases. Thus after the initial reduction of the fresh sample, the lower level of oxygen

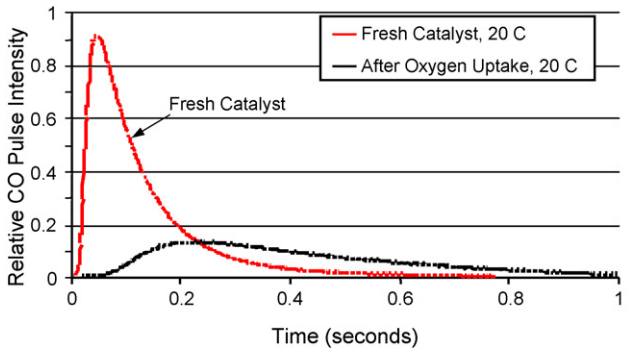

Fig. 17. CO pulses over a fresh catalyst and after CO TPR with low-temperature oxygen uptake, sample AB1.

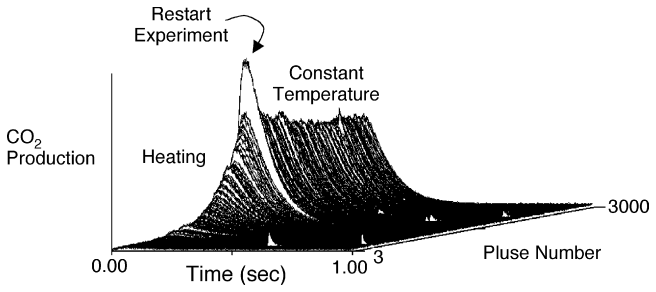

Fig. 18. CO_2 production after re-oxidation at 20 °C obtained by pulsing CO and ramping the temperature from RT to 400 °C (1500 Pd pulses).

uptake observed by adding oxygen in the pulse mode is reproducible over multiple redox cycles. This oxidation–reduction cycle is an example of an interrogative kinetics cycle in which the end states are regenerated. The oxygen composition is changing but the underlying Pd structure remains intact.

6.3.4. Oxidation of Pd samples at 400 °C

After testing the reproducibility of the oxygen uptake experiments at 20 °C on different Pd loadings, each sample was heated to 400 °C and the oxygen uptake was determined, as before, in the vacuum pulse mode. Fig. 20 shows three typical breakthrough curves for samples prepared with 500, 750, and 2500 laser pulses. The curves show that the amount of oxygen consumed increases with Pd loading, and that the uptake dependence also depends on loading. On the sample (AB0.5) prepared with 500 laser pulses the total oxygen uptake is 2.8×10^{17} O atoms. The number of Pd atoms in the form of PdO as determined by the oxygen removed in the CO temperature-programmed reduction experiments was 3.8×10^{17} atoms. Assuming the Pd as PdO was 30% the total number of Pd atoms on AB0.5 (12.7×10^{17} atoms) then there are ≈3 O-atoms for every 13 Pd atoms after the sample has been oxidized at 400 °C.

The breakthrough curves displayed in Fig. 20 contain downward peaks that are caused by stopping and restarting the oxygen input pulse. After the O_2 input is stopped the sample is maintained at constant temperature for 10 min. Upon restarting the oxygen input, the oxygen consumption shows an increase, and then within a small number of pulses returns to the level preceding the halt. The increase indicates the loss of surface oxygen, and diffusion of oxygen into the Pd bulk.

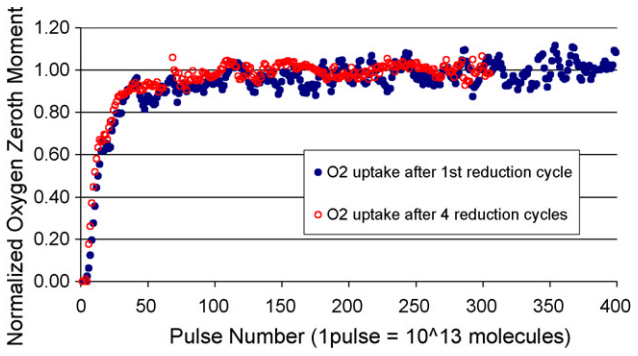

Fig. 19. Oxygen breakthrough curves at 20 °C over the same Pd/SiO_2 sample (1500 Pd pulses) after separate reduction cycles.

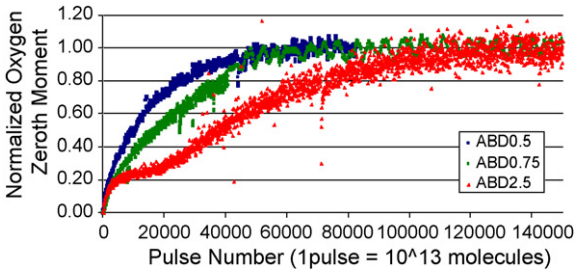

Fig. 20. Oxygen breakthrough curves at 400 °C for different Pd loadings.

Samples were oxidized in an O_2 flow (25 cm^3/min diluted in argon, O_2/Ar = 0.7) at 400 °C for 15 min. When returned to vacuum conditions the samples displayed no oxygen adsorption when exposed to a series of oxygen pulses. The oxygen response had the characteristic shape of a standard diffusion curve.

After flowing oxygen at 400 °C over the AB1 sample (prepared with 1000 laser pulses), the sample was cooled to room temperature, and a temperature-programmed reduction experiment using CO was performed. Fig. 21 compares the TPR CO_2 production for AB1 after flow oxidation at 400 °C with the TPR CO_2 production after pulsed oxidation at room temperature, but before any 400 °C oxygen treatment.

Oxygen uptake at 400 °C is ≈100× more than the oxygen uptake at 20 °C. However, TPR CO_2 production is higher on the room temperature sample, and the maximum in CO_2 occurs at a temperature 50 °C lower. Also, reduction of the 400 °C sample does not lead to the formation of lower temperature adsorption sites. After reduction with CO at 400 °C in the pulsed mode no oxygen adsorption was observed at 20 °C in vacuum pulse response experiments.

6.3.5. Oxygen uptake at intermediate temperatures

As discussed above, oxygen chemisorption at 20 °C is not observed on samples that have been oxidized at 400 °C. However, at higher temperatures oxygen uptake is substantial and increases with increasing temperature. Fig. 22 displays oxygen uptake curves obtained on the same sample (AB5) taken at 50, 100, 150, and 200 °C. The experiments were

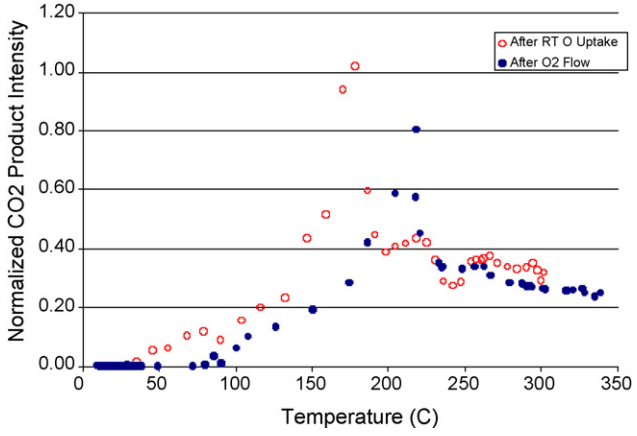

Fig. 21. TPR production of CO_2 produced by pulsing CO over AB1 after room temperature oxidation, and after O_2 flow oxidation at 400 °C.

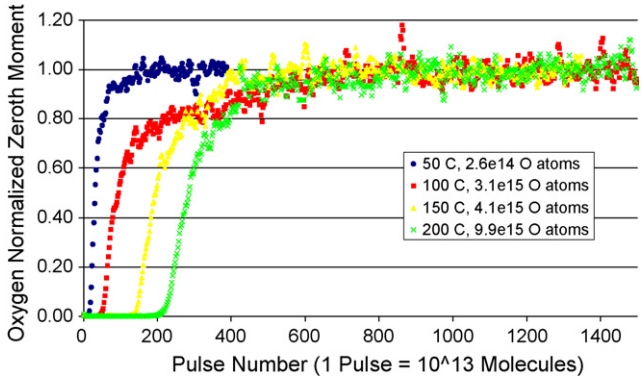

Fig. 22. Oxygen uptake curves obtained on the same sample (AB5) at different temperatures.

performed in sequence, and between uptake experiments the sample was reduced by pulsing CO at 400 °C.

6.3.6. CO_2 production at 400 °C

Fig. 23 displays the relative CO_2 production on AB0.5 and AB1.5 at 400 °C after each sample was oxidized at atmospheric pressure. As previously described, the samples were oxidized in an O_2 flow (25 cm^3/min diluted in argon, O_2/Ar = 0.7) at 400 °C for 15 min. After evacuating the reactor each sample was exposed to a long series of CO pulses at the same temperature. In both cases, CO_2 production decreases by more than 90% within 200 pulses. The total amount of CO_2 produced by AB1.5 is ≈3× the amount produced by AB0.5. After reduction both samples were cooled to 20 °C and exposed to a series of O_2 pulses. No oxygen uptake was observed.

Re-oxidation of AB0.5 and AB1 at 400 °C and pulsed reduction with CO give the same CO_2 production curves indicating that this oxidation–reduction cycle is reproducible. The cycle represents a typical interrogative state-altering cycle in which the catalyst composition changes but the underlying structure is constant.

6.3.7. Steady-state CO oxidation over different Pd/SiO_2 samples

Catalysts were operated under steady state by passing a stoichiometric mixture of CO and oxygen diluted in argon over the catalyst at various temperatures. A small portion of the

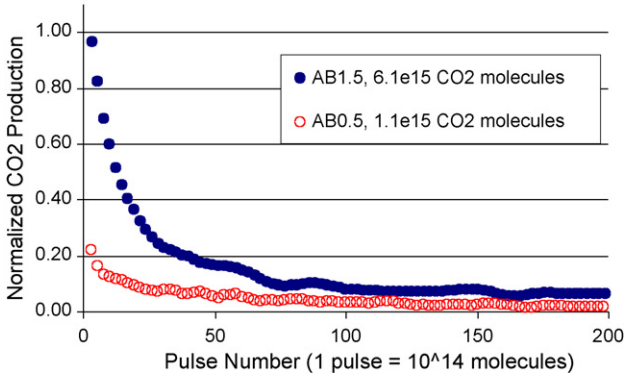

Fig. 23. CO_2 production at 400 °C on samples oxidized in an oxygen flow at 400 °C. Each sample was exposed to a series of CO pulses of equal intensity.

reactor gas phase was diverted through a needle valve to the mass spectrometer. Reactant conversion and product formation were measured by comparison with a non-reacting feed mixture passed over inert packing. From the CO conversion calculated at various temperatures an Arrhenius plot was constructed. Apparent activation energies measured over different samples ranged from 83 to 107 kJ/mol.

7. Discussion

Fig. 24 displays the scheme of kinetic experiments used in the transformation and characterization of Pd/PdO deposits on quartz particles. The numbered steps represent transformative processes (state-altering experiments), and the steps designated with red arrows represent processes that cannot be reversed (i.e., the initial catalyst cannot be regenerated from the end state). By definition, state-altering experiments involve one of the following: (1) a change in composition of one or more components, (2) a change in structure, or (3) a change in both.

7.1. Deposition

XPS analysis of higher loading samples indicated the presence of 20–30% PdO. The amount of PdO, determined from CO reduction experiments varied from sample to sample and did not show a linear dependence on Pd loading. Comparison of the oxygen pulse response with the standard diffusion curve (Fig. 11) indicates that oxygen adsorption on freshly deposited samples is negligible at room temperature. The CO response at short times is narrower than the standard diffusion curve, and at longer times its decay is slower, and it crosses over the standard diffusion curve. This behavior indicates either reversible adsorption in which the desorption rate constant is small in comparison to the adsorption rate constant, or a complex process involving more than one site with different adsorption properties.

The absence of significant oxygen adsorption is a strong indication that the surface of the fresh deposit is covered with an oxide overlayer. The presence of CO adsorption indicates the presence of a small concentration of Pd sites.

7.2. Formation of reduced Pd surface and interaction with oxygen

Catalytically active Pd materials were produced from each of the Pd/PdO deposition samples by pulsing CO and gradually increasing the temperature. The fresh deposits were highly reactive, and CO_2 production in all cases was observed at 25 °C.

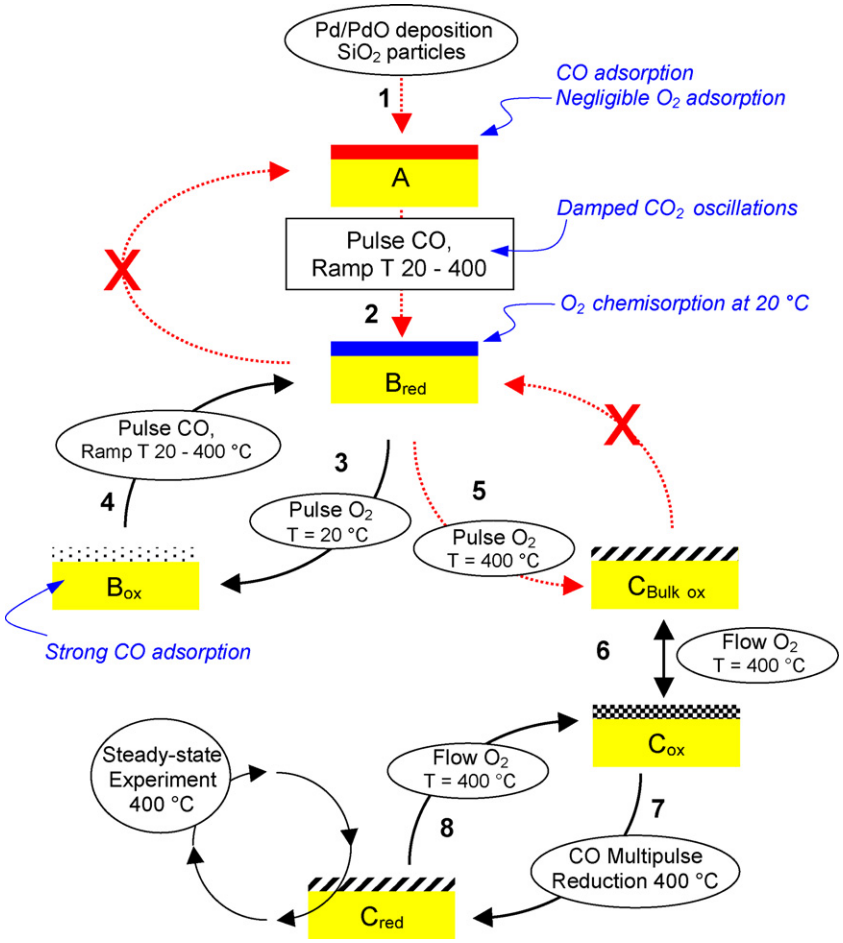

Fig. 24. Experimental roadmap illustrating the sequence of experiments used to create different kinetic states on Pd/SiO_2 catalysts prepared by atomic beam deposition. The dashed arrows represent state-altering transformations in which the initial state cannot be regenerated.

CO and O_2 pulse response data on fresh deposits indicate that the surface of Pd/PdO–SiO_2 catalysts is primarily Pd oxide with some Pd sites. The total amount of oxygen extracted during TPR experiments indicates the Pd oxide layer is probably 10 or more monolayers thick.

The CO_2 TPR spectrum displays an initial maximum between 150 and 160 °C, and then decreases rapidly. The area under the first TPR peak represents between 10 and 15% of the total CO_2 produced, and can be attributed to the reaction of pre-adsorbed CO with surface PdO. The remaining peaks show a steady decline in CO_2 production, characteristic of damped oscillations. Since the CO input is constant, the oscillatory behavior must be the result of a change in the amount of reactive oxygen. Since oxidation is occurring at the Pd/PdO surface the oscillation in oxygen composition must be accompanied by a change in the surface composition of Pd and PdO.

Oscillatory behavior in CO oxidation over Pd and Pt are well known, and have been attributed to a variety of causes including surface reconstruction [117–121], the interaction of subsurface oxygen species [122–125], and the difference in the rates of CO oxidation on metallic Pd and Pd oxide surfaces. Hendriksen et al. [126] recently reported that CO oxidation occurs more rapidly over PdO than the metallic surface, and switching between the two surfaces causes the oscillation in CO_2 production. For detailed reviews of experimental data on oscillations in heterogeneous catalytic CO oxidation and corresponding models (see Refs. [127–129]).

Typically, oscillatory behavior in CO oxidation is studied using a constant gas phase mixture of CO and O_2, and isothermal conditions. In this case, oscillations are the result of changes in surface concentrations, but both reactants are fed from the gas phase. Our results were obtained with a single gas, CO, in the TPR regime, and oxygen is supplied by the solid phase. Heuristically, every peak in the dependence presented in Fig. 12 can be viewed as a typical TPR peak related to a specific form of catalyst oxygen. CO_2 production during the first peak corresponds to the depletion of accessible surface oxygen. Then, the series of peaks that follow can be considered as resulting from reaction of CO with other forms of catalyst oxygen. Thus, abrupt changes in the amount of oxygen indicate abrupt changes in the Pd/PdO composition. Moreover, the reduction of PdO results in a volume loss of nearly 67% (based on the theoretical change in density going from PdO to Pd) and the collapse of the resulting amorphous layer anticipates an atomic reorganization in order to minimize the surface energy.

Considering the results described above we can construct a physical picture of the reduction process. In the course of the temperature rise, CO will initially produce CO_2 from the top layer. The removal of surface oxygen will generate Pd atoms, and open the top layer for reaction with CO to the second Pd oxide layer, and so on. As each new layer reacts more Pd is produced and less of the structure underneath is accessible. The total amount of CO_2 in each peak represents the amount of oxygen made available in each step.

At the molecular scale, the reduction reaction can be viewed as a reaction between CO and surface PdO in the presence of Pd. For example:

$$\begin{aligned}
&(1) && \mathrm{Pd} + \mathrm{CO} \rightleftarrows \mathrm{Pd\ CO}\\
&(2a) && (\mathrm{Pd\ PdO}) + \mathrm{CO} \rightleftarrows (\mathrm{Pd\ PdO})\mathrm{CO}\\
&(2b) && (\mathrm{Pd\ PdO})\mathrm{CO} \rightarrow \mathrm{Pd}_2 + \mathrm{CO}_2\\
&(3) && \mathrm{Pd}_2 + \mathrm{PdO} \rightarrow (\mathrm{Pd}_2\mathrm{PdO})\\
&(4a) && (\mathrm{Pd}_2\mathrm{PdO}) + \mathrm{CO} \rightleftarrows (\mathrm{Pd}_2\mathrm{PdO})\mathrm{CO}\\
&(4b) && (\mathrm{Pd}_2\mathrm{PdO})\mathrm{CO} \rightarrow \mathrm{Pd}_3 + \mathrm{CO}_2\\
&\vdots\\
&(n\mathrm{a}) && (\mathrm{Pd}_n\mathrm{PdO}) + \mathrm{CO} \rightleftarrows (\mathrm{Pd}_n\mathrm{PdO})\mathrm{CO}\\
&(n\mathrm{b}) && (\mathrm{Pd}_n\mathrm{PdO})\mathrm{CO} \rightarrow (\mathrm{Pd}_n\mathrm{Pd}) + \mathrm{CO}_2
\end{aligned}$$

In this mechanism the catalyst includes single Pd sites and mixed sites containing Pd/PdO. CO may adsorb on both sites, but CO_2 production occurs only on (Pd_nPdO) sites via rearrangement of the intermediate. Steps similar to Step (3) reflect the probability that clusters of different size are neighbors. These reactions lead to clusters or islands of enriched in palladium. The process is kinetically controlled and will depend on the initial relative concentration and spatial distribution of Pd and PdO clusters.

The correspondence between room temperature O_2 adsorption, and CO_2 production during the TPR reaction, indicates that the number of room temperature sites is related to the initial number of PdO units. As oxygen from the amorphous PdO clusters is removed, the remaining atoms will form a smaller volume cluster, with new Pd atoms being added to the cluster surface. Thus the *n*th step in the cluster forming reaction sequence may produce a high-energy, low coordination Pd^* site. The addition of small clusters to a larger cluster will produce similar low coordination sites.

The simplest interpretation of the above model is to consider that the number of reactive PdO units decreases at the same rate as the Pd cluster size increases. Increase in Pd cluster size results in trapping of PdO units. Assuming the Pd cluster is growing atom by atom, the second layer contributes 1/2 the oxygen, the third layer 1/3 the oxygen, the fourth layer 1/4, and so on.

The physico-chemical picture is expected to be more complicated than the above model depicts. For example, oxygen exchange between different levels has not been considered. However, the model captures the basic features of the data, and predicts the formation of Pd clusters with high-energy Pd sites. We expect the model to overestimate the amount of available oxygen the deeper the reduction occurs.

The process can be viewed as an example of reactive self-assembly, the combination of reaction kinetics, diffusion, and energy minimization provides the impetus. An analogous self-assembly process, recently reported in the literature, involved the formation of micrometer-scale high-aspect ratio pyramidal structures starting from polycrystalline Pd films (40–200 nm) deposited on MgO and $LaAlO_2$ substrates using pulsed laser ablation [116]. AFM images demonstrated the formation of micrometer-scale high-aspect ratio pyramidal structures after

annealing treatments in oxygen at 900 °C. This formation was only observed when the starting Pd film was polycrystalline. The results also suggest that thinner films would result in a narrower size distribution of structures. Currently we are developing deterministic and Monte-Carlo models that are based on these assumptions.

High-energy single-atom Pd sites can be expected to readily form a π-complex with O_2 and rearrange to form a highly reactive PdO site. These sites are associated with room temperature (20 °C) oxygen adsorption and low-temperature CO_2 production. We found that after catalysts are heated in a flow of oxygen at 400 °C and then reduced with CO that room temperature oxygen adsorption drops significantly, indicating a loss of high-energy sites. However, oxygen uptake still readily occurs at higher temperatures as indicated by the uptake curves shown in Fig. 22. The change in oxygen uptake as a function of temperature also indicates a distribution of adsorption sites or a change in the nature of the sites with temperature.

Comparison of the two CO response curves in Fig. 17 shows that reduction of the fresh Pd/PdO deposit changes the CO adsorption characteristics dramatically. The response after reduction is very broad in comparison to pre-reduction response, and indicates that all CO molecules in the pulse are adsorbed. This change is clear evidence that the number of CO adsorption sites has increased significantly.

The high-energy single-atom sites suggested by our results may be analogous to the single Pd atoms anchored to MgO oxygen vacancies reported by Abbet et al. They found that CO oxidation produces CO_2 on the single Pd atoms at 260 and 500 K. The reaction causes annealing of the vacancy and formation of larger clusters [130].

7.3. Reaction at elevated temperatures and pressures

Changes in the metal-enriched surface, for example metal reconstruction and morphological changes of small crystallites, are most pronounced when the catalyst is exposed to gas atmospheres, particularly under oxidizing conditions, and high temperatures [131]. In situ Raman spectroscopy [132], sum frequency generation (SFG) [133] and other techniques [134] have established that the structure and composition of a catalyst changes when exposed to a reactant gas [135–137].

In our studies, exposure of the catalyst to an atmospheric pressure flow of oxygen at elevated temperatures (400 °C) induced the collapse of fine structure created during the initial CO reduction thought to be responsible for the high-energy, low-temperature adsorption sites. For example, comparison of CO TPR experiments before and after oxygen flow indicated a decrease in total CO_2 production with the production maximum occurring almost 50 °C higher when the sample had been exposed to oxygen flow. This indicates that the unique low-temperature adsorption sites created during the initial CO reduction were no longer available. Even efforts to reduce the sample in a flow of hydrogen were unsuccessful at later re-accessing any low-temperature adsorption sites with oxygen. The kinetic properties of the catalyst towards CO pulsed reduction were found to be reproducible when exposed to numerous flow oxidations. This indicates that the evolution of the catalyst surface morphology had likely reached an endpoint early in the first oxidation.

Steady-state experiments have found that the kinetics of CO_2 formation are independent of surface orientation for palladium catalysts [85,87,89]. Under steady-state conditions when the surface coverage of CO is high, the structure-insensitivity has been attributed to the adsorptive properties on vacant sites, which is believed to dominated by repulsive interactions among CO molecules rather than any underlying metal structure [89]. When run under steady-state conditions our catalysts yielded activation energies (83–107 kJ/mol) in general agreement with that of similar palladium systems. For example on Pd(1 1 1) Engel and Ertl reported an activation energy of 104 kJ/mol at low CO coverages and 59 kJ/mol at moderate CO coverages [107] while on Pd(1 1 0) Bondzie reported and activation energy of 96.2 ± 11.8 kJ/mol [108].

The unique features created under low-pressure reaction restructuring are essentially erased upon exposure to atmospheric pressure flows. Our conclusion is that the process of sintering driven by the minimization of surface energy under atmospheric flow conditions resulted in the elimination of high-energy sites and the formation of larger, more uniform particles. In one example, TEM measurements by Chen and Schmidt revealed a dramatic increase in crystallite size when a Pt/SiO_2 catalyst was heated to 973 K in N_2 and O_2 atmospheres [138]. The sintering of palladium on supports such as Al_2O_3 [139–142], SiO_2 [139,140,143], and TiO_2 [140] when run under reaction conditions is well known and the dependence of sintering on oxidation state has been reported [144,145].

Mizsei et al., found that when thin films (4 nm) of Pd are sputtered onto a SiO_2 surface an amorphous structure is produced [109]. Upon heating in air to 500 °C, an assembly of spherical nanometer-sized (10 nm) Pd domains was observed. In general, a spherical morphology of palladium deposits is found on SiO_2 substrates after thermal treatment due to a mismatch of lattice structures [110–113]. Several studies indicate the absence of a metal–support interaction between Pd and SiO_2 [113–115].

7.4. Conclusions

A new approach for precisely tailoring the surface of complex catalytic particles at the atomic level is presented. Sub-monolayer amounts of metallic and oxide palladium were added to the surface of micron-sized quartz particles using atomic beam-deposition (ABD). The experimental system couples ABD catalyst preparation with TAP kinetic characterization in a single apparatus of original construction. This provides a new opportunity to provide atomic level catalyst design assisted by precise kinetic characterization. This approach opens new possibilities for inferring the working structure of the catalytic active site and revealing mechanistic details of complex reactions based on a battery of non-steady-state and steady-state kinetic measurements using the 'interrogative kinetics' methodology.

This methodology is illustrated using the oxidation of CO over Pd/SiO_2 catalysts. A series of catalysts of different Pd loadings were prepared using atomic beam deposition. The Pd deposits have been characterized using XPS, SEM and TEM. Deposition experiments were combined with a variety of non-steady-state TAP experiments: adsorption/reaction pulse response, temperature-programmed reaction (TPR), and steady-state experiments.

TPR experiments revealed an oscillatory behavior of CO_2 production only over untreated samples. Based on TPR and adsorption data, a qualitative model of the evolution of catalytic structure under the influence of the reactive media was proposed. Exposure to oxygen at elevated temperatures caused an irreversible collapse of the fine structure. These findings indicate the possibility of developing structural insight using kinetic information as a guide.

Acknowledgements

The authors would like to acknowledge the support of the National Science Foundation GOALI Grant CTS-0432593 for their generous support, and Rohm & Haas Company for their generous support in time and funding.

References

[1] S. Shekhtman, Doctoral Thesis, Washington University, Saint Louis, 2003.
[2] J. Gleaves, G. Yablonskii, P. Phanawadee, Y. Schuurman, Appl. Catal. A: Gen. 160 (1997) 55–88.
[3] A. Gaffney, S. Han, J. Gleaves, G. Yabolonsky, S. Shekhtman, R. Fushimi, in: Proceedings of the 18th North American Catalysis Society Meeting, Cancun, Mexico, 2003.
[4] A. Gaffney, S. Han, J. Gleaves, G. Yabolonsky, S. Shekhtman, R. Fushimi, in: Proceedings of the 226th ACS National Meeting, New York, 2003.
[5] J. Gleaves, J. Ebner, T. Kuechler, Catal. Rev.: Sci. Eng. 30 (1988) 49.
[6] S. Shekhtman, G. Yablonsky, J. Gleaves, R. Fushimi, Chem. Eng. Sci. 59 (2004) 5493–5500.
[7] J. Schwarz, C. Contescu, A. Contescu, Chem. Rev. 95 (1995) 477.
[8] S. Hong, E. Mielczarski, M. Davis, J. Catal. 134 (1992) 349.
[9] A. Berthet, A. Thomann, F. Cadete Santos Aires, M. Brun, C. Deranlot, J. Dertolini, J. Rozenbaum, P. Brault, P. Andreazza, J. Catal. 190 (2000) 49–59.
[10] B. Tardy, C. Noupa, C. Leclercq, J. Bertolini, A. Hoareau, M. Treilleux, J. Faure, G. Nihoul, J. Catal. 129 (1991) 1.
[11] M. Tanaka, M. Mukai, Y. Fujimori, M. Kondoh, Y. Tasaka, S. Usami, H. Baba, Thin Solid Films 281–282 (1996) 453–456.
[12] Z.J. Zhang, J. Huang, S. Fan, C. Liber, Mater. Sci. Eng. A 209 (1996) 5–9.
[13] H. Kwok, Thin Solid Films 218 (1992) 277–290.
[14] M. El Khakani, R. Dolbec, A. Serventi, M. Horrillo, M. Trudeau, R. Saint-Jacques, D. Rickerby, I. Sayago, Sens. Actuators B: Chem. 77 (2001) 383–388.
[15] M. Quintana, E. Haro-Poniatowasi, J. Morales, N. Batina, Appl. Surf. Sci. 195 (2002) 175–186.
[16] W. Yamaguchi, K. Yoshimura, Y. Tai, Y. Maruyama, K. Igarashi, S. Tanemura, J. Murakami, J. Chem. Phys. 112 (2000) 9961.
[17] W. Heer, Rev. Modern Phys. 65 (1993) 611.
[18] J. Bower, M. Jarrold, J. Chem. Phys. 97 (1992) 8312.
[19] I. Goldby, B. von Issendorff, L. Huipers, R. Palmer, Rev. Sci. Instrum. 68 (1997) 3327.
[20] S. Hall, M. Nielsen, A. Robinson, R. Palmer, Rev. Sci. Instrum. 68 (1997) 3335.
[21] W. Eberhardt, P. Fayet, D. Cox, A. Kaldor, R. Sherwood, D. Sondericker, Phys. Scripta 41 (1990) 892.
[22] H. Roy, P. Fayet, F. Patthey, W. Schneider, B. Delly, C. Massobrio, Phys. Rev. B 49 (1994) 5611.
[23] V. Boyakov, V. Epikhin, B. Kalin, M. Makhatov, I. Nikolaev, G. Shishkin, Sov. J. Quantum Electron. 8 (1978) 902.
[24] H. Jenniches, M. Klaua, H. Hoche, J. Kirschner, Appl. Phys. Lett. 69 (1996) 3339.
[25] S. Fahler, H. Krebs, Appl. Surf. Sci. 96–98 (1996) 61–65.
[26] T. Cheng, P. Lin, S. Chen, S. Liu, J. Juang, J. Lin, K. Wu, T. Uen, Y. Gou, R. Wang, H. Li, J. Low Temp. Phys. 131 (2003) 557.
[27] Y. Suda, H. Kawasaki, T. Ueda, T. Ohshima, Thin Solid Films 453–454 (2004) 162–166.
[28] A. Weidenkaff, C. Diecker, T. Lippert, M. Montenegro, Thin Solid Films 453–454 (2004) 406–410.
[29] N. Xu, L. Li, H. Lin, J. Wu, A. Wu, J. Sun, Z. Ying, P. Wang, Phys. Lett. A 320 (2004) 297–301.
[30] A. Serventi, R. Dolbec, M. El Khakani, R. Saing-Jacques, D. Rickerby, J. Phys. Chem. Solids 64 (2003) 2097–2103.
[31] M. Klimczak, A. Kopia, R. Chielowski, J. Jusinski, I. Suliga, Mater. Chem. Phys. 81 (2003) 558–561.
[32] J. Ebner, J. Gleaves, US Patent 4,626,412 (1986).
[33] Y. Schuurman, J. Gleaves, J. Ebner, M. Mummey, New Dev. Select. Oxid. II (1994) 203.
[34] Y. Schuurman, J. Gleaves, Ind. Eng. Chem. Res. 33 (1994) 2935–2941.
[35] Y. Schuurman, J. Gleaves, Catal. Today 33 (1997) 25–37.
[36] E. Kondratenko, O. Buyevskaya, M. Baerns, J. Mol. Catal. A: Chem. 158 (2000) 199–208.
[37] F. Majunke, M. Baerns, Catal. Today 20 (1994) 53–59.
[38] S. Shekhtman, G. Yablonsky, J. Gleaves, R. Fushimi, Chem. Eng. Sci. 58 (2003) 4843–4859.
[39] A. Gaffney, S. Han, J. Gleaves, G. Yabolonsky, S. Shekhtman, R. Fushimi, Invited lecture at the Catalysis Society of Metropolitan New York, 2003.
[40] G. Gayko, D. Wolf, V. Kondratenko, M. Baerns, J. Catal. 178 (1998) 441–449.
[41] Y. Schuurman, C. Marquez-Alvarez, V.C.H. Kroll, C. Mirodatos, Catal. Today 46 (1998) 185–192.
[42] Y. Schuurman, C. Mirodatos, Appl. Catal. A: Gen. 151 (1997) 305–331.
[43] G. Centi, F. Trifiro, G. Busca, J. Ebner, J. Gleaves, Faraday Discuss. Chem. Soc. 87 (1989) 215–225.
[44] G. Golinelli, J. Gleaves, J. Mol. Catal. 73 (1992) 353–369.
[45] J. Gleaves, G. Centi, Catal. Today 16 (1993) 69.
[46] E. McCullagh, N. Rigas, J. Gleaves, B. Hodnett, Appl. Catal. A: Gen. 95 (1993) 183.
[47] B. Kubias, U. Rodemerck, H. Zanthoff, M. Meisel, Catal. Today 32 (1–4) (1996) 243–253.
[48] U. Rodemerck, B. Kubias, H. Zanthoff, G. Wolf, M. Baerns, Appl. Catal. A: Gen. 153 (1997) 217–231.
[49] D. Dowell, J. Gleaves, Y. Schuurman, Stud. Surf. Sci. Catal. 110 (1997) 199–208.
[50] P. Mills, H. Randall, J. McCracken, Chem. Eng. Sci. 54 (1999) 3709–3721.
[51] J. Gleaves, A. Sault, R. Madix, J. Ebner, J. Catal. 121 (1990) 202–218.
[52] G. Creten, D. Lafyatis, G. Froment, J. Catal. 154 (1995) 151–162.
[53] D. Coulson, P. Mills, K. Kourtakis, P. Wijnen, J. Lerou, L. Manzer, Stud. Surf. Sci. Catal. 75 (1993) 2015.
[54] G. Creten, F. Kopinke, G. Froment, Can. J. Chem. Eng. 75 (1997) 882–891.
[55] D. Lafayatis, G. Creten, G. Froment, Appl. Catal. 120 (1994) 85–103.
[56] B. Kartheuser, B. Hodnett, H. Zanthoff, M. Baerns, Catal. Lett. 21 (1993) 209–214.
[57] O. Buyevskaya, D. Wolf, M. Baerns, Catal. Lett. 29 (1994) 249–260.
[58] E. Mallens, J. Hoebink, G. Marin, Catal. Lett. 33 (1995) 291–304.
[59] D. Wang, O. Dewaele, A. De Groote, G. Froment, J. Catal. 159 (1996) 418–426.
[60] A. Sexton, B. Kartheuser, C. Batiot, H. Zanthoff, B. Hodnett, Catal. Today 40 (1998) 247–252.

[61] O. Dewaele, G. Froment, J. Catal. 184 (1999) 499–513.
[62] M. Fathi, F. Monnet, Y. Schuurman, A. Holmen, C. Mirodatos, J. Catal. 190 (2000) 439–445.
[63] F. Dekker, J. Nazloomian, A. Bliek, F. Kapteijn, J. Moulijn, D. Coulson, P. Mills, J. Lerou, Appl. Catal. A: Gen. 151 (1997) 247–266.
[64] Y. Mergler, J. Hoebink, B. Nieuwenhuys, J. Catal. 167 (1997) 305–313.
[65] J. Hoebink, J. Huinink, G. Marin, Appl. Catal. A: Gen. 160 (1997) 139–151.
[66] Y. Schuurman, V. Ducarme, T. Chen, W. Li, C. Mirodatos, G. Martin, Appl. Catal. A: Gen. 163 (1997) 227–235.
[67] H. Zanthoff, S. Buchholz, A. Pantazidis, C. Mirodatos, Chem. Eng. Sci. 54 (1999) 4397–4405.
[68] Y. Schuurman, Th. Decamp, J. Jalibert, C. Mirodatos, Stud. Surf. Sci. Catal. (1999) 133–140.
[69] H. Zanthoff, S. Buchholz, Catal. Lett. 49 (1997) 213–217.
[70] A. Hinz, A. Andersson, Chem. Eng. Sci. 54 (1999) 4407–4421.
[71] A. Martin, Y. Zhang, H. Zanthoff, M. Meisel, M. Baerns, Appl. Catal. A: Gen. 139 (1996) L11–L16.
[72] J. Ebner, J. Gleaves, T. Kuechler, T. Li, ACS Symp. Ser. 328 (1987) 189.
[73] G. Ansell, A. Diwell, S. Golunski, J. Hayes, T. Rajaram, T. Truex, A. Walker, Appl. Catal. B: Environ. 2 (1993) 81–100.
[74] R. Burch, P. Millington, A. Walker, Appl. Catal. B: Environ. 4 (1994) 65–94.
[75] C. Rottländer, R. Andorf, C. Plog, B. Krutzsch, M. Baerns, Appl. Catal. B: Environ. 11 (1996).
[76] T. Gerlach, M. Baerns, Chem. Eng. Sci. 54 (1999) 4379–4384.
[77] S. Lacombe, J. Hoebink, G. Marin, Appl. Catal. B: Environ. 12 (1997) 207–224.
[78] E. Kondratenko, O. Buyevskaya, M. Soick, M. Baerns, Catal. Lett. 63 (1999) 153–159.
[79] D. Lafayatis, G. Froment, A. Pasau-Claerbout, E. Derouane, J. Catal. 147 (1994) 552–559.
[80] G. Svoboda, J. Gleaves, P. Mills, Ind. Eng. Chem. Res. 31 (1992) 19–29.
[81] D. Statman, J. Gleaves, D. McNamara, P. Mills, G. Fornasari, Appl. Catal. 77 (1991) 45–53.
[82] O. Buyevskaya, M. Rothaemel, H. Zanthoff, M. Baerns, J. Catal. 146 (1994) 346.
[83] E. Mallens, J. Hoebink, G. Marin, Stud. Surf. Sci. Catal. 81 (1994) 205.
[84] A. van Keulen, K. Seshan, J. Hoebink, J. Ross, J. Catal. 166 (1997) 306–314.
[85] Y. Slagtern, C. Schuurman, X. Leclercq, C. Verykios, Mirodatos, J. Catal. 172 (1997) 118–126.
[86] O. Keipert, M. Baerns, Chem. Eng. Sci. 53 (1998) 3623–3634.
[87] Y. Schuurman, A. Pantazidis, C. Mirodatos, Eng. Sci. 54 (1999) 3619–3625.
[88] W. Moser, G. Rossetti, J. Gleaves, J. Ebner, J. Catal. 127 (1991) 190–200.
[89] M. Rothaemel, H. Zanthoff, M. Baerns, Catal. Lett. 28 (1994) 321–328.
[90] R. Fushimi, S.O. Shekhtman, A. Gaffney, S. Han, G.S. Yablonsky, J.T. Gleaves, Ind. Eng. Chem. Res. 44 (2005) 6310–6319.
[91] S. Shekhtman, G. Yablonsky, S. Chen, J. Gleaves, Chem. Eng. Sci. 54 (1999) 4371–4378.
[92] D. Constales, G. Yablonsky, G. Marin, J. Gleaves, Chem. Eng. Sci. 56 (2001) 133–149.
[93] G. Yablonskii, S. Shekhtman, S. Chen, J. Gleaves, Ind. Eng. Chem. Res. 37 (1998) 2193–2202.
[94] S. Shekhtman, G. Yablonsky, J. Gleaves, R. Fushimi, Chem. Eng. Sci. 59 (2004) 5493–5500.
[95] Y. Schuurman, V. Kroll, P. Ferreira-Aparicio, C. Mirodatos, Catal. Today 38 (1997) 129–135.
[96] G.S. Yablonsky, M. Olea, G. Marin, J. Catal. 216 (2003) 120–134.
[97] G.S. Yablonsky, S.O. Shekhtman, S. Chen, J.T. Gleaves, Ind. Eng. Chem. Res. 37 (1998) 2193–2202.
[98] S.O. Shekhtman, G.S. Yablonsky, Ind. Eng. Chem. Res. 44 (2005) 6518–6522.
[99] D. Constales, G.S. Yablonsky, G.B. Marin, J.T. Gleaves, Chem. Eng. Sci. 59 (2004) 3725–3736.
[100] G. Yablonsky, S. Shekhtman, P. Phanawadee, J. Gleaves, Catal. Today 64 (2001) 227–231.
[101] A. Eppler, G. Rupprechter, L. Guczi, G. Somorjai, J. Phys. Chem. B 101 (1997) 9973–9977.
[102] S. Foltyn, In: D.A. Payne, J.C. Bravman (Eds.), Laser Ablation for Materials Synthesis, p. 205, Mater. Res. Soc. Symp. Proc., vol. (1990) 191.
[103] Z. Paszti, G. Peto, Z. Horvath, A. Karacs, L. Guczi, J. Phys. Chem. B 101 (1997) 2109.
[104] R. Klingeler, P. Bechthold, M. Neeb, W. Eberhardt, Rev. Sci. Instrum. 73 (2002) 1803–1808.
[105] U. Heiz, A. Sanchez, S. Abbet, W.-D. Schneider, J. Am. Chem. Soc. 121 (1999) 3214–3217.
[106] U. Heiz, F. Vanolli, A. Sanchez, W. Schneider, J. Am. Chem. Soc. 120 (1998) 9668–9671.
[107] T. Engel, G. Ertl, J. Chem. Phys. 69 (3) (1978) 1267–1281.
[108] V. Bondzie, P. Kleban, D. Browne, J. Vac. Sci. Technol. A 11 (4) (1993) 1946–1950.
[109] J. Mizsei, J. Voutilainen, S. Saukko, V. Lantto, Thin Solid Films 391 (2001) 209–215.
[110] D. Kochubey, S. Pavlova, B. Novgorodov, G. Kryukova, V. Sadykov, J. Catal. 161 (1996) 500–506.
[111] X. Xu, J. Szanyi, Q. Xu, D. Goodman, Catal. Today 21 (1994) 57–69.
[112] S. Tanaka, F. Mizukami, S. Niwa, M. Toba, K. Maeda, H. Shimada, K. Kunimori, Appl. Catal. A: Gen. 229 (2002) 165–174.
[113] W. Shen, M. Okumura, Y. Matsumura, M. Haruta, Appl. Catal. A: Gen. 213 (2001) 225–232.
[114] R. Hicks, A. Bell, J. Catal. 91 (1985) 104–115.
[115] W. Shen, M. Olumura, Y. Matsumura, M. Haruta, Appl. Catal. A: Gen. 213 (2001) 225–232.
[116] S. Aggarwal, A. Monga, S. Perusse, R. Ramesh, V. Ballarotto, E. Williams, B. Chalmala, Y. Wei, R. Reuss, Science 287 (2000) 2235–2237.
[117] G. Ertl, P.R. Norton, J. Rustig, Phys. Rev. Lett. 49 (1982) 177.
[118] M.P. Cox, G. Ertl, R. Imbihl, Phys. Rev. Lett. 54 (1985) 1725.
[119] R. Imbihl, M.P. Cox, G. Ertl, J. Chem. Phys. 84 (1986) 3519.
[120] M. Eiswirth, G. Ertl, Surf. Sci. 177 (1986) 90.
[121] M. Eiswirth, P. Moller, K. Wetzl, R. Imbihl, G. Ertl, J. Chem. Phys. 90 (1989) 510.
[122] S. Ladas, R. Imbihl, G. Ertl, Surf. Sci. 219 (1989) 88.
[123] M.R. Bassett, R. Imbihl, J. Chem. Phys. 93 (1990) 811.
[124] N. Hartmann, K. Krischer, R. Imbihl, J. Chem. Phys. 101 (1994) 6717.
[125] V.A. Bondzie, P. Kleban, D.J. Dwyer, Surf. Sci. 347 (1996) 319.
[126] B. Hendriksen, S. Bobaru, J. Frenken, Catal. Today 105 (2005) 234–243.
[127] G.S. Yablonskii, V.I. Elokhin, V.I. Bykov, A.N. Gorban, Kinetic models of catalytic reactions, in: R. Compton (Ed.), Comprehensive Chemical Kinetics, vol. 32, Elsevier Science, Amsterdam, 1991.
[128] M.M. Slin'ko, N.I. Jaeger, Oscillating Heterogeneous Catalytic Systems, Elsevier Science, Amsterdam, 1994.
[129] G.S. Yablonskii, V.I. Elokhin, Kinetic models of heterogeneous catalysis, in: J.A. Thomas, K.I. Zamaraev (Eds.), Perspective in Catalysis, Blackwell Sci., 1992, pp. 191–249.
[130] U. Heiz, A. Sanchez, S. Abbet, W.-D. Schneider, Chem. Phys. 262 (2000) 189–200.
[131] M. Che, C. Bennett, Adv. Catal. 36 (1989) 55–172.
[132] H. Knozinger, G. Mestl, Topics Catal. 8 (1999) 45.
[133] G. Somorjai, G. Rupprechter, J. Phys. Chem. B 103 (1999) 1623.
[134] J. Thomas, G. Somorgai, Topics Catal. 8 (1999), special issue on 'In-situ Characterization of Catalysts'.
[135] G. Centi, F. Trifiro, J.R. Ebner, V.M. Franchetti, Chem. Rev. 88 (1988) 55.
[136] J. Haber, Stud. Surf. Sci. Catal. 110 (1997) 1–106.
[137] C. Bennett, Adv. Catal. 44 (1999) 329.
[138] M. Chen, L. Schmidt, J. Catal. 55 (1978) 348–360.
[139] K. Muto, N. Katada, M. Niwa, Appl. Catal. A: Gen. 134 (1996) 203–215.
[140] T. Chang, J. Chen, C. Yeh, J. Catal. 96 (1985) 51.
[141] R.F. Hicks, H. Qi, M.L. Young, R.G. Lee, J. Catal. 122 (1990) 295.
[142] F.H. Ribeiro, M. Chow, R.A.D. Betta, J. Catal. 146 (1994) 537.
[143] B. Min, A. Santra, D. Goodman, Catal. Today 85 (2003) 113–124.
[144] J.J. Chen, E. Ruckenstein, J. Catal. 69 (1981) 254.
[145] H. Shinjoh, H. Muraki, Y. Fujitani, Stud. Surf. Sci. Catal. 71 (1991) 617.